Femtosecond near-field spectroscopy of single quantum dots

Christoph Lienau[a], Tobias Guenther[a], Thomas Unold[a], Kerstin Mueller[a] and Thomas Elsaesser[a]

[a] Max-Born-Institut für Nichtlineare Optik und Kurzzeitspektroskopie, Max-Born-Straße 2A, D-12489 Berlin, Germany;

ABSTRACT

Excitonic and spin excitations of single semiconductor quantum dots currently attract attention as possible candidates for solid state based implementations of quantum logic devices. Due to their rather short decoherence times in the picosecond to nanosecond range, such implementations rely on using ultrafast optical pulses to probe and control coherent polarizations. We combine ultrafast spectroscopy and near-field microscopy to probe the nonlinear optical response of a *single* quantum dot on a femtosecond time scale. Transient reflectivity spectra show pronounced oscillations around the quantum dot exciton line. These oscillations reflect phase-disturbing Coulomb interactions between the excitonic quantum dot polarization and continuum excitations. The results show that although semiconductor quantum dots resemble in many respects atomic systems, Coulomb many-body interactions can contribute significantly to their optical nonlinearities on ultrashort time scales.

1. INTRODUCTION

Our insight into the structure, function and dynamics of atomic, molecular, biological and solid-state nanostructures has been influenced strongly during the last two decades by two complementary and novel experimental tools, i.e., by scanning probe microscopy and ultrafast optics. The techniques of scanning probe microscopy (1), in particular scanning tunneling microscopy (STM) and atomic force microscopy (AFM), enable one to image the structure of surfaces on an atomic and even sub-atomic (2) scale and give information about the local electronic density of states. STM techniques offer the unique ability to manipulate the position of single atoms with sub nanometer precision and to assemble new structures on a nanoscale (3; 4). Dynamic processes on surfaces, however, can only be studied on a time scale given by the mechanical scan speed of the raster probe, i.e. typically on a millisecond time scale.

Optical techniques, on the other hand, are inherently diffraction limited in spatial resolution to the scale of the wavelength of the light, i.e., to about 0.5 μm in the visible range. In combination with ultrashort light pulses, optics allows to probe structural changes on femtosecond time scales. This makes ultrafast spectroscopy a unique tool for probing the elementary dynamics of electronic and nuclear motion in atomic, molecular and solid state systems. It is the ideal technique for the time-resolved study of chemical reaction dynamics (5; 6) and of the dynamics of electronic excitations in solid state media (7).

A particularly interesting research perspective lies in a combination of scanning probe microscopy and ultrafast optics to spatially resolve the ultrafast dynamics of optical excitations on ultrashort, nanometer length scales. During the last decade, scientists have embarked on different strategies to attain this goal. The combination of a scanning tunneling microscope with ultrashort light pulses offers ultimate, nanometer spatial resolution; yet, experimentally, has so far been proven difficult (8; 9). An alternative concept relies on using the nano-optical techniques that have been developed during the last decade, e.g. aperture-based (10; 11; 12) or apertureless, scattering-type (13; 14; 15) near-field microscopy, to break the diffraction limit and localize ultrashort light pulses to spatial dimensions of the order of 10 to 100 nm. Ultrafast nano-optics is currently a rapidly expanding field of research, as the newly developed experimental tools have the potential to probe and manipulate the dynamics of optical excitations of single nanostructures (16; 17; 18; 19). This allows to eliminate ensemble averaging, so far unavoidable in conventional far-field ultrafast experiments.

It is the aim of this article, to introduce a novel experimental approach, combining near-field optics and femtosecond pump-probe spectroscopy, to probe the nonlinear optical response of single nanostructures on ultrafast time scales. This technique is implemented to study the coherent polarization dynamics and optical nonlinearity

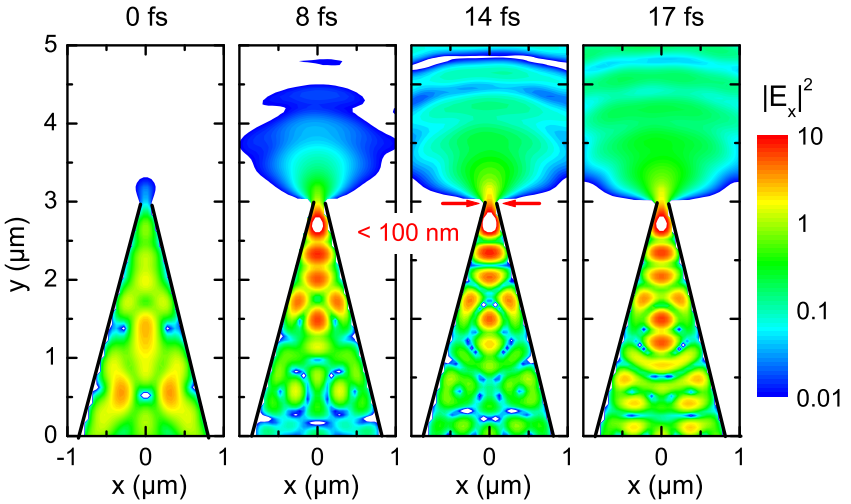

Figure 1. Two-dimensional FDTD simulation of the spatio-temporal evolution of a 10-fs light pulse at a center wavelength of 810 nm propagating through a tapered, metalized fiber probe of 100-nm aperture diameter. The field intensity $|E_x(x, y, t)|^2$ is displayed on a logarithmic intensity scale at four different instants in time. Around t =14 fs the pulse center reaches the aperture, generating an ultrashort near-field light spot directly below the aperture. Note the strong back reflection of the pulse inside the fiber. The metal coating is assumed to be a perfect conductor.

of a single semiconductor quantum dot. Analyzing transient reflectivity spectra, we directly demonstrate the effects of many-body Coulomb interactions on the excitonic polarization dynamics. The paper is organized as follows. In section 2, the experimental techniques applied in this study are introduced. Section 3 summarizes briefly some basic properties of interface quantum dots. The experimental results and their analysis are presented in section 4. A summary and some conclusions are given in section 5.

2. ULTRAFAST NANO-SPECTROSCOPY

A prerequisite for probing the dynamics of optical excitations on a nanometer scale in real space is the ability to generate and/or probe light spots with a temporal duration in the femtosecond range and nanometer spot sizes. A straightforward approach relies on transmitting ultrafast lasers through nanometer-sized apertures in nontransparent metal films. In the direct vicinity of the aperture, i.e., in its near field, the spatial resolution is defined by the dimension of the aperture, rather than by diffraction. The resolution can thus be increased by sufficiently decreasing the size of the aperture. If the aperture is fabricated at the tip of, e.g., a metal-coated tapered optical fiber, it can be raster-scanned across the sample surface, using conventional techniques of scanning probe microscopy (1). Near-field optical images are then generated by recording the transmitted or reflected light as a function of tip position. This approach is illustrated in figure 1. It depicts a two-dimensional finite difference time domain (FDTD) simulation (20) of the propagation of a 10 fs light pulse with a center wavelength of 810 nm through a metal-coated near-field fiber probe with a 100-nm aperture diameter (21). The spatial distribution of the field intensity $|E_x(x, z)|^2$ is shown on a logarithmic scale at four different instants in time. Around t =14 fs the pulse center reaches the aperture. A near-field light spot with a lateral dimension given by the aperture size is generated directly below the aperture. For a 100-nm aperture, its energy is about 3 orders of magnitude smaller than that of the incident pulse coupled into the fiber taper and this energy decreases strongly with decreasing aperture size. With current technology, aperture sizes down to about 30–40 nm can be fabricated, but the transmission coefficient is typically less than 10^{-4} (22; 23).

Since many semiconductor nanostructures are grown on non-transparent substrates, using a reflection geometry is often desirable. In metal-coated tapers, however, most of the incident pulse energy is back-reflected inside the taper. This makes it difficult to detect optical signals induced by the localized near-field light spot in a reflection geometry. Since many semiconductor nanostructures are grown on non-transparent substrates,

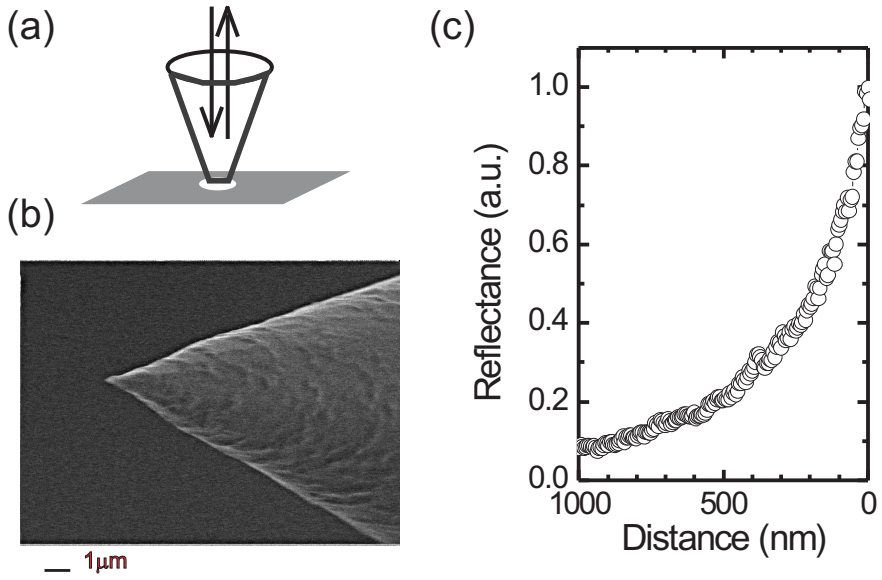

Figure 2. (a) Schematic illustration of the illumination/collection mode. (b) Scanning electron microscopy image of a etched uncoated near-field fiber probe. (c) Dependence of the reflected light detected in illumination/collection mode on the tip-to-sample distance.

using a reflection geometry is often desirable. In designing high spatial resolution experiments on semiconductor nanostructures, it is important that high optical quality semiconductor quantum wells (QWs), wires (QWRs) and dots (QDs) are often buried at a depth of 50–100 nm below the sample surface in order to avoid nonradiative recombination effects. Thus, even if an ideal point-like dipole source was used, the spatial resolution would be limited to about 1.5 - 2 times the depth, i.e., to about 100–200 nm. This also means that the amplitude of the evanescent fields generated near the surface the has decreased substantially when interacting with the buried semiconductor nanostructure.

Therefore, a slightly different approach is used in our experiments. We replace the metal-coated fiber probe by an uncoated, etched single mode optical fiber taper with a cone angle of about 30°. Tube etching (24) is used to reduce the surface roughness and improve the optical quality of the taper (figure 2). These uncoated tips are used in an illumination/collection geometry (figure 2a), detecting the light that is reflected back into the taper. This detection geometry is particularly sensitive to the local surface reflectivity, as can be seen from the pronounced decrease of the reflected light intensity with increasing tip-to-sample distance (figure 2(c)). The reflected intensity decreases by a factor of 2 within the first 150 nm. An approximately exponential distance dependence with a decay length of 250 nm, free of interference oscillations is observed for good quality tapers. 3D FDTD simulations (25) show that in the presence of a semiconductor, almost all of the incident pulse energy is adiabatically guided into a spot with a diameter of about 250 nm at the very end of the taper. In illumination/collection geometry, the spatial resolution is further improved since the light passes twice through the aperture. It can reach less than 150 nm or about $\lambda/5$ (26). The FDTD simulations also show that a large fraction of the locally reflected light is coupled back into the tapered fiber. Experimentally, we find that for GaAs samples about 1% of the light coupled into the fiber is collected in this geometry. This high transmission and collection efficiency makes such uncoated fiber probes particularly well suited for semiconductor nano-spectroscopy. Also, due to its pronounced distance dependence, the intensity of the locally reflected light can be used to sensitively sense the tip-to-sample distance with an accuracy of $+/-2$ nm. In our experiments, the reflected light is used for a sensitive, contact-free distance regulation setup, avoiding the mechanical strain that is sometimes found in shear-force based feedbacks (27).

When using these tapered fiber probes for femtosecond time-resolved spectroscopy, the temporal broadening of light pulses during propagation due to group-velocity dispersion has to be considered. For a bandwidth-limited Gaussian input pulse of duration τ_{in}, the output pulse length τ_{out} after propagation through a dispersive

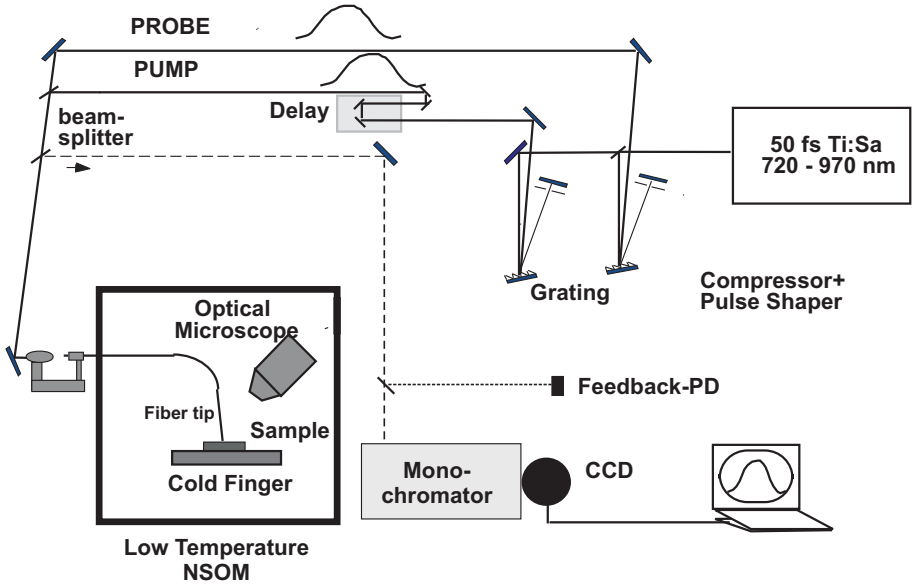

Figure 3. Schematic setup of the near-field pump-probe spectrometer (28; 12). Pump and probe pulses are derived from a 50 fs, 80 MHz repetition rate Ti:sapphire oscillator. The pulses are spectrally and temporally shaped in two independent compressor units in order to reach less than 200 fs time resolution at the exit of the fiber tip. In the illumination/collection-mode, pump and probe pulses are coupled into a near-field fiber probe and the reflected light is collected through the same fiber, spectrally dispersed in a monochromator and detected with a CCD camera. The fiber probe is raster-scanned across the sample which is mounted on the cold finger of a helium flow cryostat (29)

material of length L is given by $\tau_{out} = \tau_{in}\sqrt{1 + 4|k_d|^2 L^2/\tau_{in}^4}$. The group velocity dispersion (GVD) parameter $k_d = \partial^2 k/\partial\omega^2$, with k being the wavevector and ω the angular frequency. Higher order dispersion is neglected in this formula. For quartz single mode fibers at a laser wavelength around 800 nm, $k_d \simeq 100$ ps^2/km. In a typical, 100-cm long quartz single mode fiber, a 50 fs input pulse is stretched to about 4 ps. Thus, a GVD precompensation setup must be introduced before the fiber in order to add a negative GVD that compensates the positive GVD of the fiber. We use a grating compressor (30) (figure 3) and typically achieve a time resolution of less than 100 fs for a 40-cm-long fiber taper and less than 200 fs for 100-cm-long fibers. The achieved time resolution is mainly limited by higher order dispersion inside the optical fiber, which can not be compensated with this grating compressor. With unamplified laser pulses taken from mode-locked oscillators, the distortion of the pulse spectrum due to self-phase modulation is generally negligible.

A schematic illustration of the near-field pump-probe setup used in our experiments is shown in figure 3. Both pump and probe pulses are derived from a modelocked Ti:sapphire oscillator providing pulses with a length of about 50 fs pulses that are tunable in the wavelength range from 810 to 870 nm. The laser works at a repetition rate of 80 MHz and gives an average power of up to several hundred of milliwatt. The laser output is split into a pump and a probe beam. Each of these beams travels through a separate grating setup for spectral selection and precompensation of group velocity dispersion. Both pump and probe pulses are coupled into an uncoated near-field fiber probe. The probe light reflected from the sample is locally collected through the same fiber. The sample is mounted on the cold finger of a helium flow cryostat (29). For spectrally resolved pump-probe experiments, the collected light is dispersed in a 0.5-m monochromator yielding a spectral resolution of 60 μeV. The experiments are performed at low probe laser powers of only about 100 nW coupled into the near-field fiber, requiring a high detection sensitivity. The collected light is therefore detected with a high-sensitivity liquid-nitrogen-cooled CCD camera. The signal-to-noise ratio of the CCD detection used in this setup is approximately two times higher than the shot noise limit.

The spatial resolution that is obtained with this near-field pump-probe setup is illustrated in figure 4, showing a spatial map of the nonlinear pump-laser induced change in reflectivity of a single GaAs quantum wire (QWR) (28). The map is recorded at room temperature using a 100 fs probe laser pulse with a photon energy of 1.45

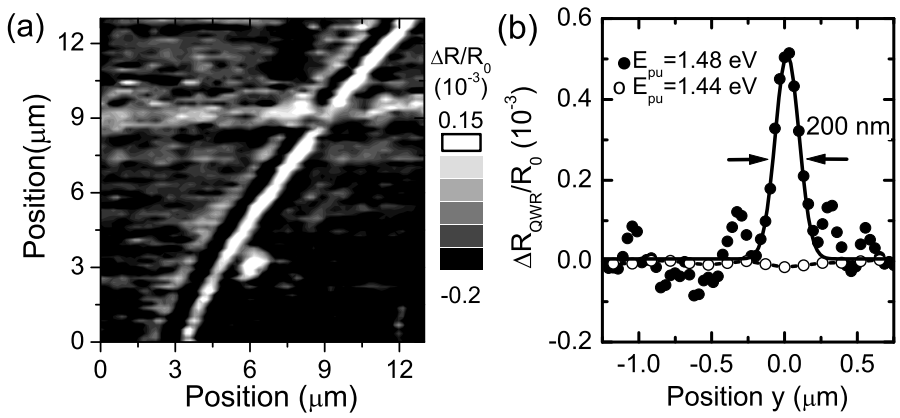

Figure 4. (a) Spatial map of the nonlinear pump-induced change in reflectivity of a single GaAs quantum wire. The map is recorded at room temperature with a probe laser set to 1.45 eV at the center of the QWR absorption resonance. A pump laser at 1.52 eV generates electron-hole pairs in the embedding quantum well. Trapping of carriers into the QWR bleaches the QWR absorption and decreases the reflectivity. (b) Spatial variation of the change in reflectivity along a line perpendicular to the quantum wire axis at a probe energy of 1.46 eV. The closed circles show data for resonant quantum wire excitation with a pump laser at E_{pu} =1.48 eV, demonstrating 200 nm spatial resolution. For off-resonant excitation at E_{pu} =1.44 eV the nonlinear signal vanishes (open circles).

eV, the center of the QWR absorption resonance. A pump laser pulse, arriving 10 ps before the probe laser, generates electron-hole pairs in the quantum well surrounding the QWR. Trapping of carriers into the QWR bleaches the QWR absorption and thus decreases the reflectivity. The local pump-induced change in QWR reflectivity is clearly resolved in figure 4(a). The temporal dynamics of the QWR reflectivity reveal an ultrafast trapping of carriers into the QWR (28)and allow to time resolve the optically-induced nonequilibrium carrier transport along the quantum wire (31).

3. INTERFACE QUANTUM DOTS

An important QD model system are thin semiconductor quantum wells (QW). In quantum wells, local monolayer height fluctuations at the interfaces (interface roughness) and fluctuations of the alloy composition (alloy disorder) are unavoidable (figure 5(a)). The resulting disordered potential leads to the localization of excitons in single "interface" quantum dots with a confinement energy of about 10 meV (figure 5(b)). This disorder gives rise to a pronounced inhomogeneous broadening of far-field optical spectra. In experiments with high spatial and spectral resolution, however, the smooth, inhomogeneously broadened photoluminescence (PL) spectra break up into narrow emission spikes from a few localized excitons (32; 33; 34; 26; 35; 36). This makes nano-optical techniques with high spectral resolution particularly well suited for studies of single QDs.

The linear optical properties of interface QDs resemble in many aspects those of atomic systems. At low temperatures, the excitonic lines display a narrow homogeneous linewidth of 30–50 μeV, in agreement with measured dephasing times of 20–30 ps. The QDs show a discrete absorption spectrum (34) and a fine structure splitting due to the spatial asymmetry of the monolayer islands. The temperature dependence of the exciton linewidth and the fine structure of these emission line has been thoroughly investigated (34; 37). The center-of-mass wave function of localized excitons in interface quantum dots typically extends over several tens of nm. This results in large QD dipole moments of 50–100 Debye and a particularly strong coupling of these excitons to light (38; 39). This makes interface quantum dots a particularly interesting model system for nonlinear spectroscopy of single quantum dots.

Much information about the underlying disorder potential and about the localization length of the excitonic wave functions is obtained from a statistical analysis of the autocorrelation function of such near-field spectra (35; 40). Specifically, such experiments reveal excitonic level repulsion as a robust correlation between localized

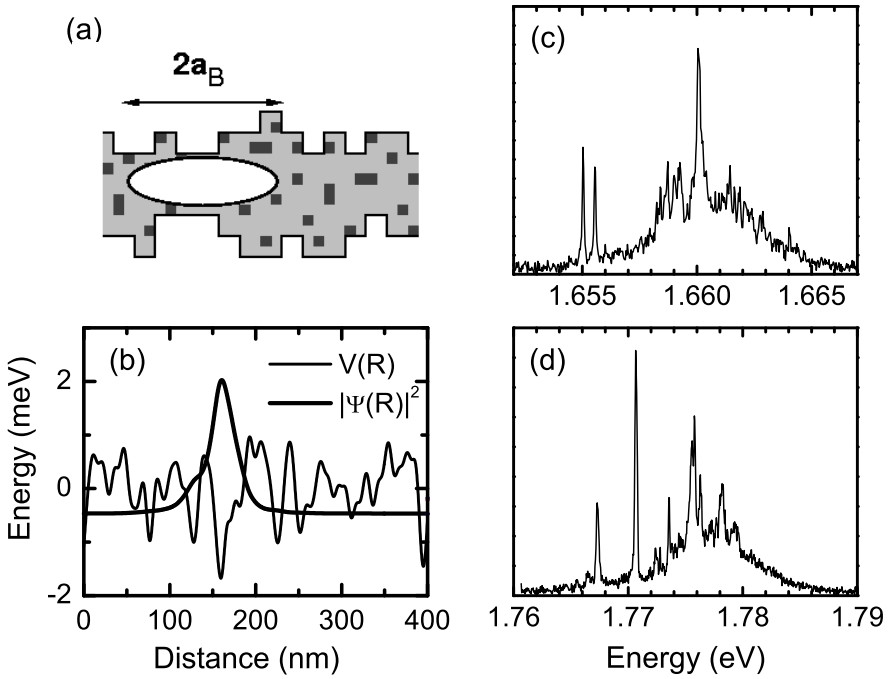

Figure 5. (a) Disorder in quantum wells arises from spatial fluctuations of the local quantum well thickness (interface roughness) and of the quantum well composition (alloy disorder). (b) Schematic illustration of the effective disorder potential $V(\mathbf{R})$ and of a localized excitonic center-of-mass wave function $|\Psi(\mathbf{R})|^2$. (c,d) Representative near-field PL spectra (T =12K) of (c) a 5.1 nm thick and (d) a 3.3 nm thick (100) GaAs QW.

exciton states with spatially overlapping wave functions and allow to estimate the correlation length of the underlying disorder potential.

In this work, we investigate a sample consisting of 12 single QW layers of different thicknesses grown on a (100) GaAs substrate. The QW layers are separated by AlAs/GaAs short period superlattice barriers, each formed by nine AlAs and GaAs layers with a total thickness of 23.8 nm. Here, we investigate the top seven QWs with thicknesses of 3.3 to 7.1 nm. The layers are buried at distances between 40 and 211 nm below the surface. Growth interruptions of 10 s at each interface lead to a large correlation length of the QW disorder potential and to the formation of interface quantum dots (QD). The growth interruptions are kept short in order to avoid a monolayer splitting of the macroscopic PL spectra and to minimize the incorporation of impurities at the interfaces.

In figures 5(c) and (d) representative low temperature (T =12 K) near-field PL spectra are shown for the 3.3 and 5.1 nm thick (100) GaAs QW. The spectra reveal clearly the emission from excitons localized in interface quantum dots. The linewidth of the sharp resonances is limited by the spectral resolution of 100 μeV. The spectra are recorded at an excitation intensity of 110 nW, corresponding to an average excitation density well below one exciton per monolayer island. For excitation powers between 1 and 500 nW, we find a linear intensity dependence and an excitation-independent shape of the emission spectra, indicating negligible contributions from biexcitons and charged excitons. In addition to the sharp localized exciton emission, these spectra display a spectrally broad background emission from more delocalized excitons in QW continuum states (26).

4. ULTRAFAST NONLINEAR OPTICAL RESPONSE OF SINGLE QUANTUM DOTS

The nonlinear optical properties of excitons in single interface QDs have been investigated mainly by high-resolution nonlinear spectroscopy in the frequency domain (16; 17). The third-order nonlinear response has been explained on the basis of homogeneously broadened two-level systems, in analogy to descriptions of atomic

systems. On the other hand, it is well known that Coulomb interactions play an important role for ultrafast optical nonlinearities of higher dimensional systems, such as quantum wells and wires. This raises the question how transient many-body interactions arising from multiexcitonic interactions (41) and/or nonresonant optical excitations of the QD and its environment [e.g., neighboring QDs (42)] affect the QD optical nonlinearities and their ultrafast dynamics. Since such couplings are difficult to probe and/or control in ensembles, time-resolved studies of single QD nonlinearities are desirable.

Knowledge about the effects of many-body interactions on the optical nonlinearities of single QDs is particularly important in the light of recent proposals to use excitonic excitations of single QDs as basic building blocks for quantum information processing in solids (42; 41). Since the decoherence times of excitonic excitations are comparatively short, in the range of 10 ps to 1 ns, such implementations rely on controlling excitonic nonlinearities on an ultrafast, femtosecond time scale, much shorter than the excitonic decoherence time. Controlled many-body interactions, e.g. via dipole-dipole coupling (42), are essential for coupling excitons in neighboring quantum dots, i.e., for implementing controlled quantum gates. Uncontrolled many-body interactions with carriers in the environment of the QD, on the other hand, effectively couple the QD excitons to a surrounding bath and thus may be an important source of decoherence.

Here, the first femtosecond study of the nonlinear optical response of a single QD is reported. By analyzing transient reflectivity spectra from single QDs, we directly probe the dynamics of the coherent excitonic polarization in the presence of nonequilibrium carriers excited in the environment of the QD. We show that excitation-induced dephasing by Coulomb interactions with continuum excitations is the dominant nonlinearity of the QD exciton on an ultrafast time scale. This presents an important step forward in probing and manipulating coherent QD polarizations, which is of fundamental importance for semiconductor-based implementations of quantum information processing.

In this section, we first describe how QD nonlinearities are probed in near-field reflectivity measurements and then analyze the dynamics of the QD nonlinearities. From these experiments, the radiative recombination rate of different quantum dots is extracted and their dipole moment is inferred. Then, the dynamics of the QD polarization in the presence of nonequilibrium carriers are discussed and excitation-induced dephasing is identified as the dominant QD nonlinearity on an ultrafast time scale.

4.1. Near-field reflectivity spectra of single quantum dots

In our experiments, we probe the QD nonlinearity by measuring the spectrum of a probe laser locally reflected from the QD sample. Here the effect of the the excitonic QD polarization on the detected spectrum, i.e., the generation of the nonlinear reflectivity signal is described.

Our experimental concept is outlined in figure 6(a). A spectrally broad femtosecond laser, centered around the QW absorption, is coupled into the near-field fiber probe. The probe laser light reflected from the sample is collected by the same fiber probe, dispersed in the monochromator and detected with the CCD camera. This steady-state reflectivity spectrum $R_0(\omega_{det})$ contains weak spectrally narrow resonances from single QD transitions (figure 6(a)). A second, blue-shifted pump laser creates carriers in QW continuum states. This nonequilibrium carrier concentration affects the QD spectrum and thus gives rise to a modified probe reflectivity $R(\omega_{det})$. Differential probe reflectivity spectra $\Delta R(\omega_{det}, \Delta t)/R_0 = [R(\omega_{det}, \Delta t) - R_0(\omega_{det})]/R_0(\omega_{det})$ are recorded at a fixed spatial position of the near-field tip as a function of the time delay Δt between pump and probe pulses. To probe the nonlinear optical response from single quantum dots, the high spatial resolution of the near-field technique is needed for two reasons. First, the combined spatial and spectral resolution allows to isolate single QD resonances (figure 5). Second, the relative amplitude of the QD resonance in $R_0(\omega_{det})$ scales, in first approximation, inversely proportional to the square of the spatial resolution. Thus improving the resolution from 1 μm to 100 nm increases the weak nonlinear QD signal by two orders of magnitude.

Specifically, in our experiments, pump pulses centered at 1.675 eV with an energy of 1.5 fJ and a repetition rate of 80 MHz create less than five electron-hole pairs in QW states, corresponding to an excitation density of $5 \cdot 10^9 \mathrm{cm}^{-2}$. The 1 fJ probe pulses of 18 meV bandwidth are centered at 1.655 eV, around the QW absorption resonance. Figure 6(b) depicts a differential reflectivity spectrum $\Delta R(E_{det})$ at a time delay of 30 ps in the low energy region of the 5.1 nm QW absorption spectrum. It displays a single spectrally sharp resonance at exactly

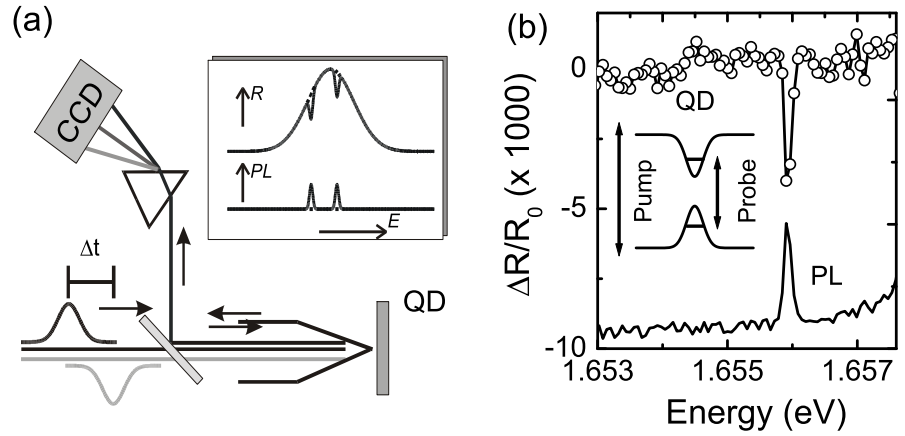

Figure 6. (a) Schematic illustration of the experimental setup and of near-field PL and reflectivity spectra of the QD sample. (b) Near-field PL spectrum of a single QD (solid line) and differential reflectivity spectrum $\Delta R/R_0$ at Δt =30 ps. PL and ΔR are recorded with identical pump pulses centered at 1.675 eV, exciting electron-hole pairs in 2D continuum states. The 100 nW probe pulses of 19 meV bandwidth are centered at 1.655 eV, around the QD absorption resonance. Inset: Schematic energy diagram.

the same spectral position E_{QD} as the simultaneously recorded near-field PL spectrum. The large amplitude of the signal of $5 \cdot 10^{-3}$ is consistent with a spatial resolution of the experiment of 200–250 nm. Two-dimensional spatial scans indicate a resolution of 230 nm, limited by the QW-to-surface distance.

Figure 7 compares differential reflectivity $\Delta R(E_{det})$ and PL spectra recorded under similar excitation conditions for single localized excitons in five different QWs buried at distances of 95 nm to 211 nm below the surface. We very clearly observe a transition between a dispersion-like and an absorption-like line shape as the QW to surface distance is varied. This behavior of the QD line shape can be understood in the framework a local oscillator model as caused by the interference between the electric probe laser field $E_R(t)$ reflected from the sample surface and the field $E_{QD}(t)$ emitted from the QD in back direction. A fraction $E_R(t)$ of the probe laser is reflected from the sample surface and coupled back into the near field fiber probe. The probe field $E_T(t)$, transmitted into the semiconductor, induces a polarization $P_{QD}(t) = \int dt' \chi_{QD}(t') E_T(t-t')$ of the QD located at a distance d below the sample surface. Here, $E_T(t)$ and χ_{QD} denote the probe field interacting with the QD and the QD susceptibility, respectively. The QD polarization re-emits an electric field and a fraction of this field, $E_{QD}(t)$ is locally collected by the near-field probe where it interferes with $E_R(t)$. The time-integrated reflectivity $R(\omega)$ detected behind the monochromator is proportional to $|\tilde{E}_{QD}(\omega) + \tilde{E}_R(\omega)|^2 \simeq |\tilde{E}_R(\omega)|^2 + 2Re[\tilde{E}_R^*(\omega)\tilde{E}_{QD}(\omega)]$, where $\tilde{E}(\omega)$ denotes the Fourier transform of the field $E(t)$. Here, the finite monochromator resolution and the weak contribution from $|E_{QD}|^2$ has been neglected. Excitation by the pump laser affects the QD polarization and thus results in a change of the QD reflectivity. The differential reflectivity $\Delta R(\omega, \Delta t)$ represents the spectral interferogram of $\tilde{E}_R$ and $\tilde{E}_{QD}$:

$$\Delta R(\omega, \Delta t) \propto \mathrm{Re}\{\tilde{E}_R^*(\omega)[\tilde{E}_{QD}(\omega, \Delta t) - \tilde{E}_{QD,0}(\omega)]\}. \quad (1)$$

The spectral shape of this interferogram evidently depends on the QD polarization dynamics and on the phase delay between $E_{QD}(t)$ and $E_R(t)$. Treating the QD for simplicity as a point dipole and the near-field tip as a point-like emitter, the phase delay depends on the distance between quantum dot and near field tip. This interference effect is nicely seen in figure 7 and explains the transition between absorptive and dispersive line shapes. Since the QDs are buried more than 50 nm below the surface, the near-field terms of the QD dipole emission can be neglected since they decay on a typical length scale of $\lambda/(2\pi n) \simeq$35 nm ($n \simeq 3.5$ - refractive index). Based on an optical path of $4\pi nd/\lambda$, we estimate a phase change of $\pi/2$ for a change in QD-sample distance of 28 nm. This is in quite good agreement with the results of figure 7. We consider this convincing evidence for the validity of the phenomenological local oscillator model described above. Clearly a detailed

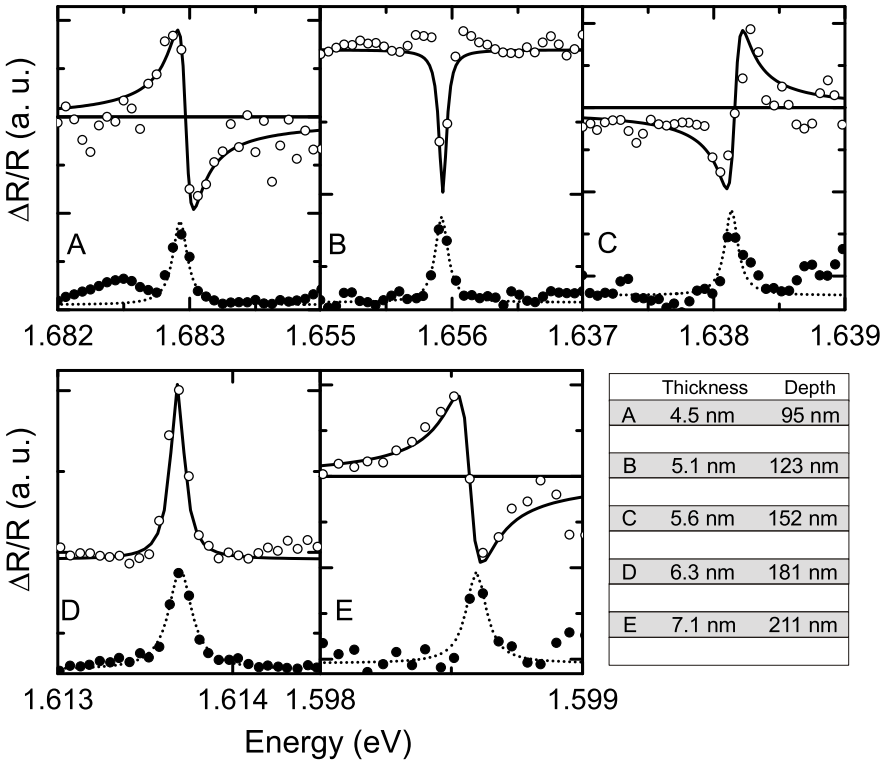

Figure 7. Differential reflectivity spectra (open circles) of five interface QDs located at different depths of 95 to 210 nm below the sample surface (see inset). The differential reflectivity spectra are compared to simultaneously recorded PL spectra. Note the transition between dispersive and absorptive line shapes.

analysis of these data, using, e.g., a Green function solution of Maxwell's equations for a realistic experimental geometry is desirable for a quantitative comparison between experiment and theory.

4.2. Exciton recombination in single quantum dots

In this section, the dynamics of the differential QD reflectivity spectra on a 100 ps time scale are analyzed. The data allow to extract the exciton lifetime and infer the QD dipole moment. Figure 8(a) shows the time evolution of $\Delta R(E_{QD})$ for three different QD resonances at 1.6598 eV (circles), 1.6614 eV (triangles) and 1.6647 eV (squares). ΔR displays a slow decay with time constants τ_{QD} of 50–150 ps. The lifetime is found to fluctuate from QD to QD. The overall trend is a decrease with increasing E_{QD}. A clear correlation between $1/\tau_{QD}$ and the magnitude of ΔR is observed.

The nonlinearities observed at sufficiently long positive Δt are easily understood on the basis of a simple two-level model for the QD nonlinearity. The pump laser creates a non-equilibrium distribution of electron-hole pairs in QW continuum states. Subsequent trapping of these carriers gives rise to a bleaching of the QD absorption and a concomitant decrease of the QD absorption. Hence, the decay time of ΔR reflects the lifetime of the individual exciton state probed. Following an earlier conjecture (34), the QD population decay is mainly dominated by radiative recombination, i.e. $\tau_{rad} \simeq \tau_{QD}$. We can then estimate the dipole moment of the individual QDs using (43; 39):

$$\frac{1}{\tau_{rad}} = n\frac{\omega^3 \cdot d_{QD}^2}{3\pi\epsilon_0\hbar c^3}. \tag{2}$$

We estimate dipole moments d_{QD} of 50 to 85 Debye for τ_{rad} between 150 and 50 ps. These values are in rather good agreement with previous estimates (18; 43). They exceed those of atomic systems by more than an order of magnitude and reflect the large spatial extension of the exciton center-of-mass wave function in

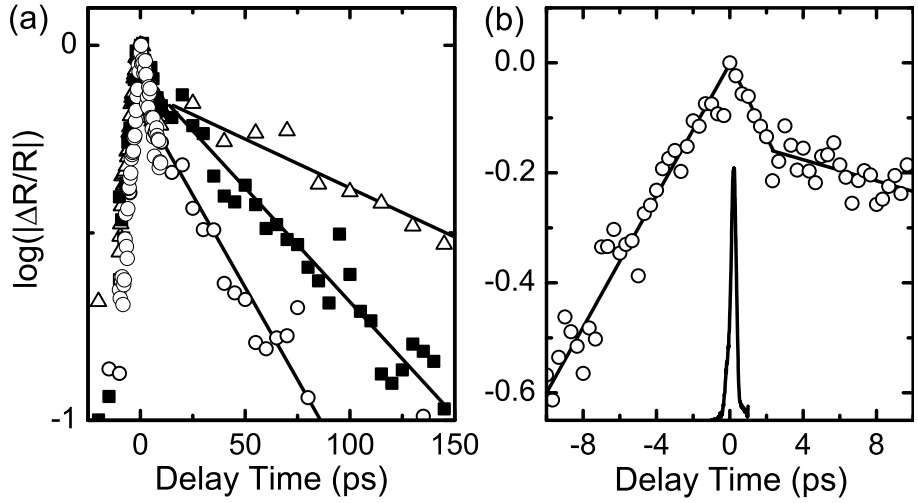

Figure 8. (a) Temporal dynamics of $\Delta R/R$ for three different QD resonances (logarithmic ordinate scale). All decays are biexponential with a slow decay time varying between 30 and 150 ps. (b) Early time $\Delta R/R_0$ dynamics of a single QD resonance. A slow rise of $\Delta R/R_0$ is observed at negative time delays. The time resolution of the experiment is 150 fs, as indicated by the cross-correlation measurement (solid line around Δt=0).

these QDs. Near-field autocorrelation spectra indicate an exciton localization length of about 40-50 nm. Due to the statistical nature of the disorder potential, the exciton localization length and thus the dipole moment and radiative recombination rate varies quite strongly from QD to QD, as seen in figure 8(b). Theoretical models of localized excitons in disordered quantum wells (44) yield comparable results.

4.3. Coherent quantum dot polarization dynamics and excitation induced dephasing

In this section, the dynamics of the QD reflectivity on a time scale of few ps is discussed. After nonresonant femtosecond excitation of carriers in continuum states, we observe, unlike in atomic systems, transient differential reflectivity spectra with pronounced oscillatory structure around the QD exciton resonance. These oscillations reflect the perturbation of the free induction decay of the coherent QD polarization by transient many-body interactions.

Figure 8(b) plots the dynamics of QD reflectivity change time delays between -10 ps and +10 ps. The time evolution of $\Delta R(E_{QD}, \Delta t)$ shows an 8-ps rise at negative delay times, much slower than the 150-fs cross correlation of pump and probe pulses. A biexponential decay is found at positive delays. The fast decay time of about 6 ps is similar for all different QD's investigated, whereas the decay time of the slow component varies from dot to dot. The reflectivity $\Delta R_t(\Delta t) = \int dE_{det} \Delta R(E_{det}, \Delta t)$, spectrally integrated over an energy interval of 2 meV around the QD resonance, vanishes at negative delay times and shows a slow exponential decay at $\Delta t > 0$. The spectral characteristics of the differential reflectivity are markedly different at positive and negative delays (figure 9). At negative delays, pronounced spectrally symmetric oscillations around the excitonic resonance are observed. Their oscillation period decreases with increasing negative time delay. At large positive delays, the spectra show a bleaching of the QD resonance.

To account for this behavior, one has to consistently describe the dynamics of the field $E_{QD}(t)$ radiated from the coherent QD polarization $P_{QD}(t)$. We phenomenologically describe the QD as an effective two-level system with a ground, no-exciton state $|0\rangle$, and an excited one-exciton state $|1\rangle$. Within the density matrix formalism, $P_{QD}(t)$ is given as $P_{QD}(t) = d^*_{QD}\rho_{01} + c.c.$, where d_{QD} denotes the QD dipole moment and ρ_{01} the microscopic QD polarization (45). Then, the well known Bloch equations hold and ρ_{01} obeys the equation of motion

$$\frac{\partial}{\partial t}\rho_{01}(t) = -i\omega_{QD}\rho_{01}(t) + i(1 - 2n_{QD})\omega_R - \gamma\rho_{01}(t), \tag{3}$$

with exciton energy ω_{QD}, dephasing rate γ, exciton population n_{QD} and generalized Rabi frequency ω_R.

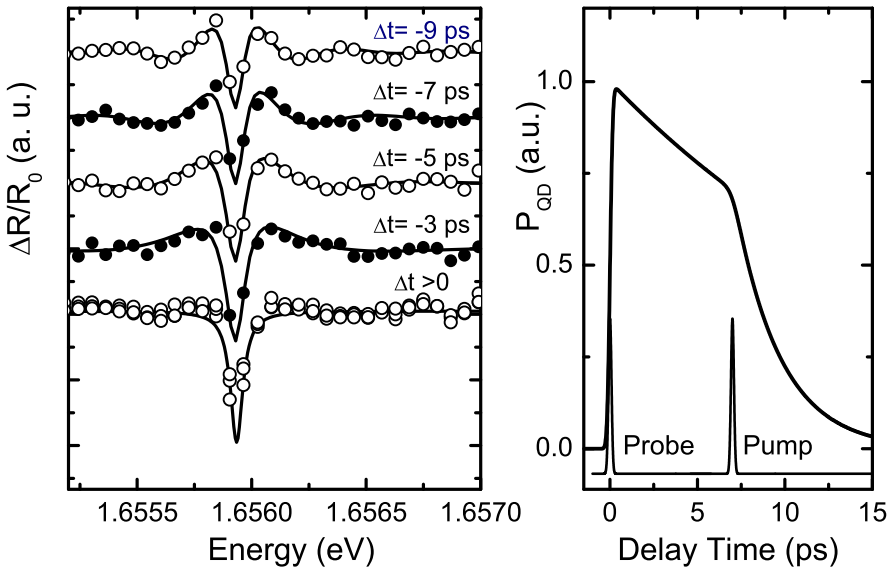

Figure 9. (a) Near-field $\Delta R/R_0$ spectra (circles) at different delay times Δt. The spectra at $\Delta t < 0$ display pronounced spectral oscillations around the excitonic resonance. The solid lines shows simulated spectra for the perturbed free induction decay of the coherent QD polarization assuming T_2=15 ps. (b)Dynamics of $P_{QD}(t)$ extracted from the time-dependent near-field $\Delta R/R_0$ spectra.

In the absence of a pump laser, the resonant probe laser impulsively excites a coherent QD polarization that then decays with the dephasing rate γ. The re-emitted field interferes with the reflected probe laser field, giving rise to a Lorentzian QD line shape in $R_0(\omega)$ (figure 6). The fact that we observe a linewidth that is limited by our monochromator resolution of about 60μeV gives a lower limit for the QD dephasing time of $T_2 = 1/\gamma > 15$ps.

Such a line shape is only observed under weak excitation conditions. For strong excitation, Rabi oscillations (18; 46) influence the polarization and population dynamics and affect the QD line shape. The experiments reported in this paper are all performed in the weak excitation limit with a probe pulse area of less than 0.4π. In additional experiments, that will be discussed elsewhere, clear Rabi oscillations are observed for resonant QD excitation and time-resolved detection of the induced biexcitonic QD nonlinearity.

The transient spectral oscillations around the QD exciton resonance at negative time delays indicate that this free induction decay of the $P_{QD}(t)$ is perturbed by the presence of the pump laser. In semiconductors, such oscillations have so far only been observed for higher dimensional system, e.g., studies of transient QW nonlinearities (47; 48). In our experiments, the off-resonant pump does not directly interact with the QD dipole but creates electron-hole pairs (density n_{QW})in the QW continuum. Thus many-body interactions perturb the free induction decay of $P_{QD}(t)$.

The spectra at $\Delta t < 0$ are quantitatively described by assuming that an excitation-induced dephasing (49), i.e., an increase in γ due to the interaction between ρ_{01} and n_{QW} is the leading contribution to the QD nonlinearity at early times. Coulomb scattering between the QD dipole and the initial nonequilibrium carrier distribution in the QW causes this additional fast damping of ρ_{01}. In the frequency domain, this excitation-induced dephasing leads to oscillatory structures in the spectrum with a period determined by the time delay between probe and pump. The solid lines in figure 9(a) are calculated from equation (3) by assuming that the probe-induced QD polarization $P_{QD}(t)$ decays initially with an effective dephasing time $T_2 = 15$ ps, decreasing to $T_{EID} = 3$ ps after the arrival of the pump laser (figure 9(b)). Such an excitation-induced dephasing model accounts quantitatively for the the transient oscillations and this analysis allows to extract the QD polarization dynamics.

A detailed theoretical analysis of the data was performed on the basis of the semiconductor Bloch equations in the mean-field approximation (19). In first approximation, the excitation-induced dephasing rate should increase linearly with the pump-induced nonequilibrium carrier concentration n_{QW} in QW continuum states.

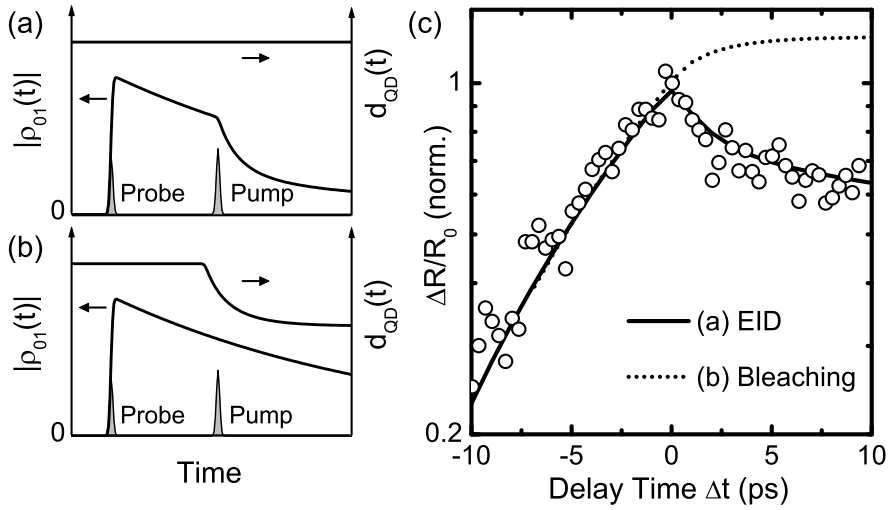

Figure 10. Simulation illustration of two models assuming (a) bleaching (a) and excitation-induced dephasing as the dominant QD nonlinearity. (c) Experimental $\Delta R(\omega_{QD})/R_0$ dynamics and simulations based on the two models.

Such a phenomenological model for the dephasing rate $\gamma = 1/T_2 + \gamma_1 \cdot n_{QW}$ was included in the simulations and good agreement between experiment and theoretical simulation was obtained. The theoretical simulations show clearly the importance of excitation-induced dephasing to the perturbed free induction decay.

The assumption of a density-dependent dephasing rate can also explain the fast decay of the differential reflectivity at early positive delay times (figure 8(b)). We assume that n_{QW} decays on a time scale of about 3 ps. This decay is most likely due to carrier trapping into QD states. Then, the initial fast differential reflectivity decay reflects the transition from a QD nonlinearity dominated by excitation-induced dephasing to a nonlinearity dominated by exciton bleaching due to the population relaxation into the QD. The slow decay of the differential reflectivity on a time scale of tens of ps then reflects the population lifetime, i.e., the electron-hole pair recombination time in the individual QDs. It is determined by radiative recombination and inversely proportional to the square of the QD dipole moment, as discussed above.

This model for the QD nonlinearity allows to quantitatively describe the dynamics of the differential reflectivity at both positive and negative delay times (figure 10). It accounts for the transient spectral oscillations at negative delay times and reproduces the biexponential decay at positive delay times.

The experimental spectra probe reflect the dynamics of the QD polarization $P_{QD}(t)$, which is given as the product of the dipole moment d_{QD} and the microscopic polarization ρ_{01}. Thus, one may speculate that a change in the oscillator strength model of the quantum dot may account for the observed spectra (50). Such an oscillator strength model is inconsistent with our experimental results. Within such a model one expects an increase in $\Delta R(E_{QD}, \Delta t)$ at positive delay times on the time scale of the switch-off time of the dipole moment (figure 10). In contrast, an initial decay is observed, in agreement with the assumption of a nonlinearity that is dominated by excitation induced dephasing.

These results show quite clearly that although single quantum dots resemble in many respect atomic systems, Coulomb many-body interactions contribute significantly to their optical nonlinearities on ultrashort time scales. Such many-body interactions have to be taken into account as important additional dephasing mechanisms. On the other hand, the now established ability to probe the dynamics of coherent polarization of single excitons in real time improves our understanding of such interactions. This is important for optimizing quantum dot geometries and excitonic excitations with their environment.

Also, the strong Coulomb and light-matter interactions in excitonic systems open up new and very interesting ways for a controlled ultrafast manipulation of coherent QD polarizations, e.g. via dipole-dipole interactions of

neighboring quantum dots (42). This is highly relevant for semiconductor-based implementations of quantum information processing.

5. CONCLUSION

In summary, we have described and demonstrated a novel experimental technique, combining near-field microscopy and femtosecond pump-probe spectroscopy, to probe the nonlinear optical response of single nanostructures. The techniques provides a spatial and temporal resolution of 200 nanometer and 100 femtoseconds, respectively. Detecting the spectrally resolved reflected probe laser light with a high-sensitivity CCD camera allows to temporally resolve the optical nonlinearity of a *single* semiconductor quantum dot. The high sensitivity of the pump-probe technique demonstrated in this work makes it a powerful tool for probing nanoscale optical nonlinearities of a wide class of materials, e.g, organic semiconductors or photochromic molecules. It will be interesting to further improve the spatial resolution of the near-field pump-probe technique, e.g. by using apertureless metallic probes. This opens the way to performing nonlinear optical spectroscopy on a length scale of 10 nm.

6. ACKNOWLEDGMENT

High-quality semiconductor samples for this work have been provided by Soheyla Eshlaghi and Andreas D. Wieck (Ruhr-Universität Bochum), Richard Nötzel and Klaus Ploog (Paul-Drude-Institut Berlin). Theoretical support by Markus Glaneman, Vollrath Martin Axt and Tilmann Kuhn (Universität Münster) is gratefully acknowledged.

This project has been financially supported by the Deutsche Forschungsgemeinschaft (SFB 296) and the European Union through the EFRE and SQUID programs.

References

[1] R. Wiesendanger, *Scanning Probe Microscopy*, Springer, Berlin, 1998.

[2] F. J. Giessibl, S. Hembacher, H. Bielefeldt, and J. Mannhart, "Subatomic features on the silicon (111)-(7*7) surface observed by atomic force microscopy," *Science* **289**, pp. 422–425, 2000.

[3] D. M. Eigler and E. K. Schweizer, "Positioning single atoms with a scanning tunnelling microscope," *Nature* **344**, pp. 524–526, 1990.

[4] H. C. Manoharan, C. P. Lutz, and D. M. Eigler, "Quantum mirages formed by coherent projection of electronic structure," *Nature* **403**, pp. 512–515, 2000.

[5] G. R. Fleming, *Chemical Applications of Ultrafast Spectroscopy*, Oxford University Press, Oxford, 1986.

[6] A. H. Zewail, "Femtochemistry: Atomic-Scale Dynamics of the Chemical Bond," *J. Phys. Chem. A* **104**, pp. 5660–5694, 2000.

[7] J. Shah, *Ultrafast spectroscopy of semiconductors and semiconductor nanostructures*, Springer, Berlin, 2 ed., 1998.

[8] V. Gerstner, A. Thon, , and W. Pfeiffer, "Thermal effects in pulsed laser assisted scanning tunneling microscopy," *J. Appl. Phys.* **87**, pp. 2574–2580, 2000.

[9] V. Gerstner, A. Knoll, W. Pfeiffer, A. Thon, , and G. Gerber, "Femtosecond laser assisted scanning tunneling microscopy," *J. Appl. Phys.* **88**, pp. 4851–4859, 2000.

[10] E. Betzig and J. K. Trautman, "Near-field optics: microscopy, spectroscopy, and surface modification beyond the diffraction limit.," *Science* **257**, pp. 189–195, 1992.

[11] M. A. Paesler and P. J. Moyer, *Near-field optics*, Wiley, New York, 1996.

[12] C. Lienau and T. Elsaesser, "Spatially and temporally resolved near-field scanning optical microscopy studies of semiconductor quantum wires," *SEMICONDUCTORS AND SEMIMETALS* **67**, pp. 39–107, 2000.

[13] F. Zenhausern, Y. Martin, and H. K. Wickramasinghe, "Scanning interferometric apertureless microscopy: optical imaging at 10 angstrom resolution.," *Science* **269**, pp. 1083–1085, 1995.

[14] B. Knoll and F. Keilmann, "Near-field probing of vibrational absorption for chemical microscopy," *Nature* **418**, pp. 134–137, 1999.

[15] R. Hillenbrand, T. Taubner, and F. Keilmann, "Phonon-enhanced light–matter interaction at the nanometre scale," *Nature* **418**, pp. 159–162, 2002.

[16] N. H. Bonadeo, G. Chen, D. Gammon, D. S. Katzer, D. Park, and D. G. Steel, "Nonlinear Nano-Optics: Probing One Exciton at a Time," *Phys. Rev. Lett.* **81**, pp. 2759–2762, 1998.

[17] N. H. Bonadeo, J. Erland, D. Gammon, D. Park, D. S. Katzer, and D. G. Steel, "Coherent Optical Control of the Quantum State of a Single Quantum Dot," *Science* **282**, pp. 1473–1476, 1998.

[18] T. H. Stievater, X. Li, D. G. Steel, D. Gammon, D. S. Katzer, D. Park, C. Piermarocchi, , and L. J. Sham, "Rabi Oscillations of Excitons in Single Quantum Dots," *Phys. Rev. Lett.* **81**, pp. 2759–2762, 2001.

[19] T. Guenther, C. Lienau, T. Elsaesser, M. Glanemann, V. M. Axt, T. Kuhn, S. Eshlaghi, , and A. D. Wieck, "Erratum: Coherent Nonlinear Optical Response of Single Quantum Dots Studied by Ultrafast Near-Field Spectroscopy [Phys. Rev. Lett. 89, 057401 (2002)]," *Phys. Rev. Lett.* **89**, p. 179901, 2002.

[20] K. S. Kunz and R. J. Lübbers, *The finite difference time domain method for electromagnetics*, CRC Press, Boca Raton, USA, 1993.

[21] R. Müller and C. Lienau, "Propagation of femtosecond optical pulses through uncoated and metal-coated near-field fiber probes," *Appl. Phys. Lett.* **76**, pp. 3367–3369, 2000.

[22] A. Naber, D. Molenda, U. C. Fischer, H.-J. Maas, C. Höppener, N. Lu, , and H. Fuchs, "Enhanced Light Confinement in a Near-Field Optical Probe with a Triangular Aperture," *Phys. Rev. Lett.* **89**, p. 210801, 2002.

[23] K. Matsuda, T. Saiki, S. Nomura, M. Mihara, , and Y. Aoyagi, "Near-field photoluminescence imaging of single semiconductor quantum constituents with a spatial resolution of 30 nm," *Appl. Phys. Lett.* **81**, pp. 2291–2293, 2002.

[24] P. Lambelet, A. Sayah, M. Pfeffer, C. Philipona, and F. Marquis-Weible, "Chemically etched fiber tips for near-field optical microscopy: a process for smoother tips.," *Appl. Optics* **37**, pp. 7289–7292, 1998.

[25] R. Müller and C. Lienau, "Three-dimensional analysis of light propagation through uncoated near-field fibre probes," *J. Microscopy* **202**, pp. 339–346, 2001.

[26] F. Intonti, V. Emiliani, C. Lienau, T. Elsaesser, R. Nötzel, , and K. H. Ploog, "Near-field optical spectroscopy of localized and delocalized excitons in a single GaAs quantum wire," *Phys. Rev. B* **63**, pp. 075313, 1–5, 2001.

[27] H. D. Robinson, M. G. Müller, B. B. Goldberg, and J. L. Merz *Appl. Phys. Lett.* **72**, pp. 2081–2083, 1998.

[28] T. Guenther, V. Emiliani, F. Intonti, C. Lienau, T. Elsaesser, R. Nötzel, and K. H. Ploog, "Femtosecond near-field spectroscopy of a single GaAs quantum wire," *Appl. Phys. Lett.* **75**, pp. 3500–3502, 1999.

[29] G. Behme, A. Richter, M. Süptitz, , and C. Lienau, "Vacuum near-field scanning optical microscope for variable cryogenic temperatures," *Rev. Sci. Instrum.* **68**, pp. 3458–3465, 1997.

[30] O. Martinez, "3000-times grating compressor with positive group velocity dispersion," *IEEE J. Quantum Electron.* **23**, pp. 59–64, 1987.

[31] V. Emiliani, T. Guenther, C. Lienau, R. Nötzel, , and K. H. Ploog, "Ultrafast near-field spectroscopy of quasi-one-dimensional transport in a single quantum wire," *Phys. Rev. B* **61**, pp. R10583–R10586, 2000.

[32] K. Brunner, G. Abstreiter, G. Böhm, G. Tränkle, , and G. Weimann, "Sharp-Line Photoluminescence and Two-Photon Absorption of Zero-Dimensional Biexcitons in a GaAs/AlGaAs Structure," *Phys. Rev. Lett.* **73**, pp. 1138–1141, 1994.

[33] H. F. Hess, E. Betzig, T. D. Harris, L. N. Pfeiffer, and K. W. West, "Near-field spectroscopy of the quantum constituents of a luminescent system," *Science* **264**, pp. 1740–1745, 1994.

[34] D. Gammon, E. S. Snow, B. V. Shanabrook, D. S. Katzer, , and D. Park, "Fine Structure Splitting in the Optical Spectra of Single GaAs Quantum Dots," *Phys. Rev. Lett.* **76**, pp. 3005–3008, 1996.

[35] F. Intonti, V. Emiliani, C. Lienau, T. Elsaesser, V. Savona, E. Runge, R. Zimmermann, R. Nötzel, , and K. H. Ploog, "Quantum Mechanical Repulsion of Exciton Levels in a Disordered Quantum Well," *Phys. Rev. Lett.* **87**, pp. 076801, 1–4, 2001.

[36] V. Emiliani, F. Intonti, C. Lienau, T. Elsaesser, R. Nötzel, and K. H. Ploog, "Near-field optical imaging and spectroscopy of a coupled quantum wire-dot structure," *Phys. Rev. B* **64**, pp. 155316, 1–9, 2001.

[37] D. Gammon, E. S. Snow, B. V. Shanabook, D. S. Katzer, and D. Park, "Homogeneous liniwidths in the optical spectrum of a single gallium arsenide quantum dot," *Science* **273**, pp. 87–90, 1996.

[38] J. R. Guest, T. H. Stievater, X. Li, J. Cheng, D. G. Steel, D. Gammon, D. S. Katzer, D. Park, C. Ell, A. Thränhardt, G. Khitrova, and H. M. Gibbs, "Measurement of optical absorption by a single quantum dot exciton," *Phys. Rev. B* **65**, pp. 241310(R), 1–4, 2002.

[39] A. Thränhardt, C. Ell, G. Khitrova, and H. M. Gibbs, "Relation between dipole moment and radiative lifetime in interface quantum dots," *Phys. Rev. B* **65**, p. 035327, 2002.

[40] G. von Freymann, U. Neuberth, M. Deubel, M. Wegener, G. Khitrova, , and H. M. Gibbs, "Level repulsion in nanophotoluminescence spectra from single GaAs quantum wells," *Phys. Rev. B* , p. 205327, 2002.

[41] P. Chen, C. Piermarocchi, , and L. J. Sham, "Control of Exciton Dynamics in Nanodots for Quantum Operations," *Phys. Rev. Lett.* **87**, p. 067401, 2001.

[42] E. Biolatti, R. Iotti, P. Zanardi, and F. Rossi, "Quantum Information Processing with Semiconductor Macroatoms," *Phys. Rev. Lett.* **85**, pp. 5647–5650, 2000.

[43] L. C. Andreani, G. Panzarini, and J. M. Gerard, "Strong-coupling regime for quantum boxes in pillar microcavities: Theory," *Phys. Rev. B* **60**, p. 13276, 1999.

[44] V. Savona, E. Runge, R. Zimmermann, F. Intonti, V. Emiliani, C. Lienau, and T. Elsaesser, "Level Repulsion of Localized Excitons in Disordered Quantum Wells," *phys. stat. sol. (a)* **190**, pp. 625–629, 2002.

[45] H. Haug and S. W. Koch, *Quantum theory of the optical and electronic properties of semiconductors*, World Scientific, Singapore, 2 ed., 1994.

[46] A. Zrenner, E. Beham, S. Stuffer, F. Findeis, M. Bichler, and G. Abstreiter, "Coherent properties of a two-level system based on a quantum-dot photodiode," *Nature* **418**, pp. 612–614, 2002.

[47] B. Fluegel, N. Peyghambarian, G. Olbright, M. Lindberg, S. W. Koch, M. Joffre, D. Hulin, A. Migus, and A. Antonetti, "Femtosecond Studies of Coherent Transients in Semiconductors," *Phys. Rev. Lett.* **59**, pp. 2588–2591, 1987.

[48] J. P. Sokoloff, M. Joffre, B. Fluegel, D. Hulin, M. Lindberg, S. W. Koch, A. Migus, A. Antonetti, and N. Peyghambarian, "Transient oscillations in the vicinity of excitons and in the band of semiconductors," *Phys. Rev. B* **38**, pp. 7615–7621, 1988.

[49] H. Wang, K. Ferrio, D. G. Steel, Y. Z. Hu, R. Binder, , and S. W. Koch, "Transient nonlinear optical response from excitation induced dephasing in GaAs," *Phys. Rev. Lett.* **71**, pp. 1261–1264, 1993.

[50] M. Joffre, "Comment on "Coherent nonlinear optical response of single quantum dots studied by ultrafast near-field spectroscopy"," *Phys. Rev. Lett.* **90**, p. 139701, 2003.